Science of the Total Environment 951 (2024) 175509

Contents lists available at ScienceDirect

Science of the Total Environment

journal homepage: www.elsevier.com/locate/scitotenv

Development and validation of an adsorption process for phosphate removal and recovery from municipal wastewater based on hydrotalcite-related materials

C. Maggetti [a], D. Pinelli [a], V. Di Federico [a], L. Sisti [a], T. Tabanelli [b], F. Cavani [b], D. Frascari [a,*]

[a] Department of Civil, Chemical, Environmental and Materials Engineering (DICAM), Alma Mater Studiorum –, University of Bologna, via Terracini 28, 40131 Bologna, Italy

[b] Dipartimento di Chimica Industriale "Toso Montanari", Alma Mater Studiorum –, University of Bologna, Viale Risorgimento 4, 40136, Bologna, Italy

HIGHLIGHTS

- Calcined pyroaurite effectively removed and recovered phosphate from wastewater.
- It resulted in high phosphate adsorption selectivity and high operational capacity.
- Performances resulted stable during 6 consecutive adsorption/desorption cycles.
- Suitable results obtained also with wastewater from hotspot of seawater intrusion.
- Scale-up from 20-cm to 60-cm column led to constant adsorption performances.

GRAPHICAL ABSTRACT

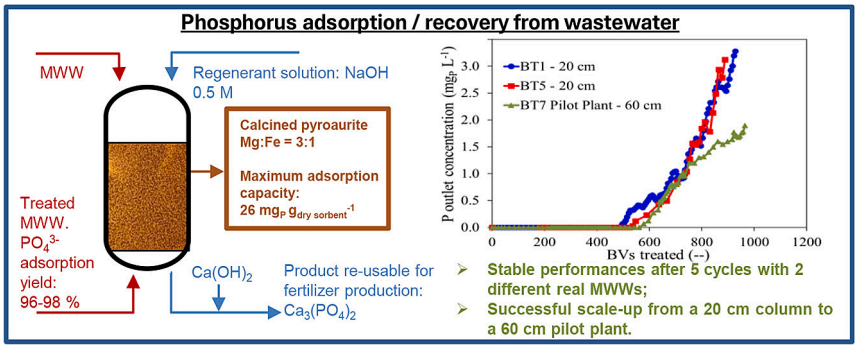

ARTICLE INFO

Keywords:
Adsorption
Hydrotalcite
Municipal wastewater
Phosphorous recovery
Pilot plant
Seawater intrusion in coastal aquifers

ABSTRACT

In the current international context characterized by the tendency to stricter limits for P concentration in treated wastewater and a strong drive towards phosphate recovery, it is crucial to develop cost-effective technologies to remove and recover phosphate from municipal wastewater (MWW). In this study, an initial screening of the phosphate adsorption performances of 9 sorbents including several hydrotalcites led to the selection of calcined pyroaurite - an innovative material composed of mixed Mg/Fe oxides - as the best-performing one. The assessment of calcined pyroaurite by means of isotherms and continuous-flow adsorption/desorption tests conducted with actual MWW resulted in a high P sorption capacity (12 $mg_P\ g^{-1}$ at the typical phosphate concentration in MWW), the capacity to treat 730 BVs at the 1 $mg_P\ L^{-1}$ breakpoint imposed by the current EU legislation, and a 93 % phosphate recovery. Calcined pyroaurite resulted in satisfactory performances also in a test conducted with a saline MWW deriving from a hotspot of seawater intrusion, a rapidly increasing phenomenon as a result of climate change. Five consecutive adsorption/desorption cycles conducted in a 20-cm column at a 5-min empty bed contact time resulted stable in terms of P adsorption/recovery performances, specific surface area and chemical structure of calcined pyroaurite. In the perspective to apply phosphate recovery with calcined pyroaurite at full scale, the process scale-up to a 60-cm packed bed - close to the column

* Corresponding author.
E-mail address: dario.frascari@unibo.it (D. Frascari).

https://doi.org/10.1016/j.scitotenv.2024.175509
Received 21 June 2024; Received in revised form 7 August 2024; Accepted 12 August 2024
Available online 13 August 2024

heights of industrial applications - resulted in stable performances. Calcium phosphate, widely used to produce phosphate-based fertilizers, can be obtained from the desorbed product by precipitation with $Ca(OH)_2$. These results point to calcined pyroaurite as a very promising material for phosphate removal and recovery from MWW and from other P-rich effluents in a circular economy perspective.

Abbreviations

As	Asymmetry factor
BET	Brunauer, Emmett and Teller surface area
BP	breakpoint
BT	breakthrough test
BV	empty bed volume of sorbent (mL)
BVs	number of bed volumes
C_L	liquid phase concentration of anions (mg L^{-1})
$C_{L,0}$, $C_{L,eq}$	initial and final (equilibrium) ion concentration in the liquid phase (mg L^{-1})
$C_{S,eq}$	final (equilibrium) PO_4-P concentration in the solid phase (sorbent) during the isotherm tests ($mg_P\ g^{1}_{dry\ sorbent}$)
$C^{\infty}_{S,i}$	maximum amount of P sorbed per unit mass of adsorbent, in the Langmuir model (mg $g^{-1}_{dry\ sorbent}$)
EBCT	empty bed contact time, ratio between resin bed volume (L) and flowrate (Lh^{-1}) used in the breakthrough test (min)
GHGs	Greenhouse gases
HETP	height equivalent to a theoretical plate
$K_{eq,i}$	equilibrium constat related to the affinity between the binding sites and the *i*-compound, in the Langmuir model (L mg_i^{-1})
$K_{F,i}$	sorption capacity in the Freundlich model ($mg_P^{1-1/n}\ L^{1/n}\ g^{-1}_{dryresin}$)
K_{Th}	Thomas rate constant (L h^{-1} mg^{-1})
m_s	mass of the dry sorbent
MWW	municipal wastewater
n_i	inverse of the sorption intensity in the Freundlich model (−)
OC	operating capacity of the sorbent ($mg_P\ g^{-1}_{dry\ sorbent}$)
v_s	superficial velocity (m h^{-1})
WWTP	wastewater treatment plant

1. Introduction

Phosphorous (P) is essential for life since it is a main nutrient in plant growth. Approximately 90 % of phosphate rock is used for food production, and the global P fertilizer use has increased from 4.6 million tons in 1961 to approximately 21 million tons in 2020. Several studies estimate that the current rate of fossil P mining (30 10^6 t_P y^{-1}) will lead to depletion of P resources within a few hundred years (Reijnders, 2014). Thus, P was listed as a critical raw material by the European Union (European Commission, 2024).

Municipal wastewaters (MWW) contain 4–12 mg L^{-1} of P (Tchobanoglous et al., 2012). While incomplete P removal from wastewater treatment plants (WWTPs) contributes to eutrophication, MWW represents a promising source for P recovery (Schoumans et al., 2015). Thus, the revised Wastewater Treatment Directive approved by the EU Parliament in April 2024 reduced the limit for WWTP discharges to 0.5 mg_P L^{-1} for WWTPs serving >150,000 people equivalent and delegated the European Commission to set a minimum rate of P recovery from MWW or sludge.

P is typically removed from wastewater by either chemical precipitation or enhanced biological removal. Both processes determine a transfer of P to sludge, from where it can be potentially recovered by struvite precipitation, or by extraction from ash if sludge is incinerated (Tchobanoglous et al., 2012). Adsorption represents a promising alternative for P removal from MWW (Bunce et al., 2018). It presents relevant advantages in comparison to chemical precipitation or biological removal: it leads to a final product usable for fertilizer manufacture, it does not lead to any additional sludge production, and it allows a full control of the effluent quality, allowing for compliance with the lower limits for WWTP discharges imposed by the new Wastewater Treatment Directive (Blaney et al., 2007; Sengupta and Pandit, 2011).

Many studies focused on the development of materials to selectively remove P from MWW by adsorption (Bunce et al., 2018). A first group of materials is represented by hybrid anion exchanger (HAIX) media, in which a strong base anion exchange resin supports a dispersion of metal oxide nanoparticles with a substantial increase in the selectivity towards P with respect to other anions of the MWW (Blaney et al., 2007; Cumbal et al., 2003; Pan et al., 2009). An effective HAIX sorbent is LayneRT, a commercial polymeric resin originally developed for Arsenic removal doped with hydrated ferric nanoparticles (Boyer et al., 2011; Pinelli et al., 2022a). LayneRT is the only material for which an adsorption-based P removal/recovery process has been scaled-up at demonstration scale (10 m^3 d^{-1} plant) and assessed by means of a complete economic analysis (Martin et al., 2013, 2018; Martin et al., 2009; Muhammad et al., 2019).

Another interesting group of materials for selective P removal from MWW is represented by Layered Double Hydroxides (LDHs), that feature alternated layers of hydroxide anions, metal cations and other anions. The intercalated anions are weakly bound, which makes them easily exchangeable. Thanks to their highly adjustable chemical composition, LDHs find application across diverse fields including catalysis, membrane separation, fuel cells, drug delivery, CO_2 capture, and adsorption (De Maron et al., 2021; Gjyli et al., 2019; Tabanelli et al., 2018). Several studies are focused on P removal from MWW using LDHs (Cheng et al., 2023; Hu et al., 2020; Keyikoglu et al., 2022; Kuzawa et al., 2006; Ogata et al., 2019). However, most of these studies were conducted with phosphate solutions in water, whereas one of the main challenges in P removal from MWW arises from the strong competition exerted by the other anions, typically present in MWW at significantly higher concentrations.

All LDHs can be calcined in the attempt to increase their mechanical strength. Calcination determines volatilization of the intercalated molecules in the structure, causing a collapse of the material into a mixed oxide form and freeing the active sites initially occupied by the volatilized ions. Nevertheless, these materials have the capability to recover the original layered structure once they are in contact with water, adsorbing intercalating ions from the water. This effect is called “hydrotalcite memory effect” (Kwon et al., 2020). Once the LDH structure is rebuilt, the ion exchange capability may be different and potentially better than that of the uncalcined material.

The general goal of this work was to develop a process for the removal and recovery of phosphate from MWW by adsorption / ion exchange on innovative sorbents, leading to a desorbed product utilizable to produce fertilizers. The specific goals of this work and the corresponding novelties were:

i) to perform a preliminary screening of different materials for P removal and recovery: the HAIX polymeric resin LayneRT, a ferric hydroxide sorbent and several LDHs, including pyroaurite, an innovative and promising Fe/Mg LDH produced internally at the University of Bologna and utilized only in two previous studies of P adsorption (Sun et al., 2014; Sun et al., 2013);
ii) to further investigate the P removal/recovery performances of the best performing material selected during the initial screening, by means of complete isotherms and continuous flow adsorption/desorption tests conducted with two distinct MWWs, including a

saline one deriving from a hotspot of seawater intrusion; conversely the vast majority of previous studies were conducted with synthetic phosphate solutions, neglecting the complex matrix effects and competition from other anions (Cheng et al., 2023; Gizaw et al., 2022; Hu et al., 2020; Sun et al., 2014);

iii) to assess the P adsorption performances, the chemical stability and the specific surface area of the best performing material during 6 continuous flow adsorption / recovery cycles conducted with actual WWTP effluents, whereas most previous studies were limited to batch isotherms or only one continuous flow adsorption test (Cheng et al., 2023; Nuryadin and Imai, 2021);

iv) to scale up the process from a 20-cm column to a 60-cm column placed in an automated pilot plant; conversely all previous studies of continuous flow P adsorption with LDHs were conducted with resin bed heights in the 0.5–10 cm range, far from the heights typical of full-scale adsorption processes (Cheng et al., 2023; Hu et al., 2020; Nuryadin and Imai, 2021).

2. Materials and methods

2.1. Characteristics of the tested adsorbents

The following 9 sorbents were investigated in this work: two commercial hydrotalcites, Pural 70 and Pural 50, provided by Sasol, tested in their commercial form and after calcination at 500 °C for 5 h; calcined Pural 70 after impregnation with Fe_2O_3; FerroSorp® Plus, a Fe(III) oxide, used in the removal of As from MWW; the commercial HAIX, LayneRT; pyroaurite, a hydrotalcite that has iron as constituent, synthesized internally at the University of Bologna, tested before and after calcination. The main features of the tested adsorbent materials, along with the procedure of pyroaurite synthesis are reported in Text S1 and Table S1, Supplementary Material.

2.2. Characteristics of the municipal wastewaters

All isotherms and continuous flow tests were conducted with two effluents of municipal WWTPs, whose main features are shown in Table 1: i) the Bologna (Italy) WWTP effluent, featuring a P concentration of 1.0 $mg_P\ L^{-1}$, consistently with the requirements of the EU Urban Wastewater Treatment Directive 91/271; and ii) the effluent of a pilot-scale membrane bioreactor that treats the saline MWW of Falconara Marittima (Italy), a hotspot of seawater intrusion. The Falconara effluent features a P concentration of 2.3 $mg_P\ L^{-1}$. As these effluents have a lower phosphate concentration than the one normally present in a municipal WWTP effluent if no P removal is implemented (EPA - U.S. Environmental Protection Agency, 2007), they were spiked with a KH_2PO_4:K_2HPO_4 solution (2:1 *w*/w) to reach the concentration of 7 $mg_P\ L^{-1}$.

2.3. Adsorption isotherms

Adsorption equilibrium isotherm tests were used for a preliminary assessment of the performances of the tested sorbents at different P concentration. 0.05 L glass vials were placed in a rotatory shaker (160 rpm, 22 °C) for 24 h, to reach equilibrium. A first group of single-point equilibrium tests was aimed at selecting the most promising P adsorption materials among those listed in section 2.1. These tests were conducted at a 2 $g\ L^{-1}$ concentration of sorbent, with Falconara WWTP effluent, a saline MWW featuring high competing anions concentration. Then, conventional multi-point isotherms were conducted with the most promising materials in the 1–15 $mg_P\ L^{-1}$ range, at a 1 $g\ L^{-1}$ concentration of sorbent, using the Bologna WWTP effluent. Experimental data were interpolated by means of the *Langmuir* and *Freundlich* models and the model parameters were assessed through least-squares, as detailed in Text S2, Supplementary Material. Details about data elaboration were described previously (Medri et al., 2022; Pinelli et al., 2022b).

Table 1
Main characteristics of the tested WWTP effluents.

Compound	Symbol	Unit	Falconara WWTP effluent	Bologna WWTP effluent
Biological Oxygen demand	BOD_5	$mg_{O2}\ L^{-1}$	42 ± 1	15 ± 2
Chemical Oxygen demand	COD	$mg_{O2}\ L^{-1}$	38 ± 5	29 ± 2
Total suspended solids	TSS	$mg\ L^{-1}$	10 ± 1	5.3 ± 0.6
Phosphate[a]	PO_4^{3-}	$mg_P\ L^{-1}$	2.3 ± 0.2	1.0 ± 0.2
Chloride	Cl^-	$mg\ L^{-1}$	311 ± 3	150 ± 12
Nitrate	NO_3^-	$mg\ L^{-1}$	2.5 ± 1.0	6.7 ± 0.5
Sulphate	SO_4^{2-}	$mg\ L^{-1}$	45 ± 1	104 ± 9
Ammonium	NH_4^+	$mg\ L^{-1}$	17 ± 2	3.9 ± 0.3
Sodium	Na^+	$mg\ L^{-1}$	214 ± 7	101 ± 8
Potassium	K^+	$mg\ L^{-1}$	24 ± 3	13 ± 2
Magnesium	Mg^{2+}	$mg\ L^{-1}$	32 ± 1	14 ± 1
Calcium	Ca^{2+}	$mg\ L^{-1}$	97 ± 9	83 ± 6
pH	pH	–	7.9 ± 0.2	7.9 ± 0.2

[a] The effluents were spiked with a KH_2PO_4:K_2HPO_4 solution (2:1 *w*/w) to achieve 7 $mg_P\ L^{-1}$.

2.4. Column packing and fluid dynamic characterization

Two packed columns were used in this work for the continuous flow P removal/recovery tests: a 30-cm column packed with 20 cm of resin bed, and a 90-cm column packed with 60 cm of resin bed - the minimum height used in industrial applications - and placed into a pilot plant featuring automatized operation and sampling. The design parameters of the lab-scale and pilot plant columns are reported in Table 2. The columns were packed with a slurry of the selected sorbent dispersed in de-ionized water following the procedure suggested by Rohm and Haas Company (Rohm and Hass Company, 2005).

The fluid-dynamic behaviour of the packed column was studied before each adsorption experiment to estimate the packing quality of the resin bed by means of three indicators: i) height equivalent of a theoretical plate (HETP), ii) reduced plate height (HETP/d_p, where d_p is the average particle diameter) and iii) asymmetry factor, defined as the ratio between the leading and tailing semi-width of the peak at 10 % of the peak height. These indicators were evaluated as illustrated previously (Frascari et al., 2016) and in Text S3, Supplementary Material. The fluid-dynamic characterization was performed by a conventional frontal analysis test carried out flowing inside the column an NaOH 2 % *w*/w (0.5 M) tracer solution with the same empty bed contact time (EBCT) applied for the adsorption tests (5 min). Electrical conductivity was measured at the column outlet with a CO11 conductivity probe (VWR, Radnor, Pennsylvania, USA).

2.5. Continuous flow adsorption/recovery breakthrough tests

In all tests, temperature was controlled at 23 ± 1 °C by recirculating water between the column's jacket and a temperature-controlled bath. 23 °C represents the maximum temperature - and therefore the least favorable condition for adsorption - typically reached by municipal wastewater in Northern Italy (Cipolla and Maglionico, 2014). During the adsorption step, wastewater was pumped downward in the column with a 5 min EBCT. Pressure drop and flow rate were measured hourly. Outlet

Table 2
Design parameters, operational conditions and performances of the breakthrough tests conducted with calcined pyroaurite and LayneRT resin in the lab-scale and pilot plants, using different MWWs.

	Test ID ➔	Lab-scale calcined pyroaurite – Bologna WWTP effluent (BT1–5)[a]	Lab-scale calcined pyroaurite – Falconara WWTP effluent (BT6)	Pilot-plant calcined pyroaurite – Bologna WWTP effluent (BT7)	Pilot plant HAIX LayneRT – Bologna WWTP effluent
Operational conditions	Column diameter (m)	0.013	0.013	0.013	0.013
	Sorbent bed height (m)	0.20	0.20	0.60	0.94
	Empty bed volume of sorbent (mL)	26.5	26.5	79.6	124.6
	mass of dry sorbent (g)	16.5	16.5	49.4	37.8
	P concentration (in the feed) ($mg_P\ L^{-1}$)	6.4	6.5	6.7	7.1
	EBCT, adsorption (min)	5.0	5.0	5.0	5.1
	Superficial velocity – adsorption phase (m h^{-1})	2.4	2.4	7.2	7.2
	Regenerant, type and concentration	NaOH 0.5 M	NaOH 0.5 M	NaOH 0.5 M	NaOH 0.5 M
	EBCT, desorption (min)	10.0	10.0	10.0	10.0
	Superficial velocity – desorption phase (m h^{-1})	1.2	1.2	3.6	3.6
Performances	Bed volumes treated @ 1 $mg_P\ L^{-1}$ BP[b]	734 ± 29	323 ± 33	729 ± 11	251 ± 10
	Bed volumes treated @ 0.5 $mg_P\ L^{-1}$ BP[b]	612 ± 56	242 ± 25	651 ± 12	229 ± 9
	P adsorption yield @ 1 $mg_P\ L^{-1}$ BP[b]	97.2 ± 0.9 %	95.8 ± 0.5 %	98.4 % ± 0.7 %	99.1 % ± 0.4 %
	Sorbent utilization efficiency @ 1 $mg_P\ L^{-1}$ BP[b]	69 ± 12 %	41 ± 11 %	55 ± 3 %	90 ± 6 %
	Overall P recovery yield @ 1 $mg_P\ L^{-1}$ BP[b]	92 %	91 %	93 %	94 %
P OC	P conc. in the desorbed product ($mg_P\ L^{-1}$)[c]	242 ± 47	233 ± 31	579 ± 58	195 ± 26
	@ $C_{L0,P}$, from BT test[d] ($mg_P\ g^{-1}$)	12.2 ± 3.4	10.7 ± 1.2	11.6 ± 0.8	6.5 ± 0.1
	@ 1 $mg_P\ L^{-1}$ BP of the BT test[e] ($mg_P\ g^{-1}$)	8.1 ± 1.2	3.8 ± 1.3	7.4 ± 0.5	5.4 ± 0.2
	Thomas model constant K_{Th} ($L\ h^{-1}\ mg_P^{-1}$)	0.013 ± 0.007	0.008 ± 0.002	0.010 ± 0.003	0.11 ± 0.02

[a] Average values from breakthrough tests BT1–5.
[b] Performance parameters were evaluated at a 1 $mg_P\ L^{-1}$ or 0.5 $mg_P\ L^{-1}$ breakpoint, as specified for each parameter.
[c] Data referred to the product solution obtained after 95 % of P desorption.
[d] P operating capacity ($mg_P\ g^{-1}_{dry\ sorbent}$) estimated at saturation in each breakthrough test; for the tests stopped before saturation, the estimate is based on the best fitting Thomas curve, extrapolated until resin saturation.
[e] P operating capacity ($mg_P\ g^{-1}_{dry\ sorbent}$) estimated at the 1 $mg_P\ L^{-1}$ BP in each breakthrough test.

samples were taken hourly. Inlet samples were taken every 3 h and the average inlet concentration was used to normalize the outlet values. Adsorption tests were stopped when about half of inlet concentration was reached in the outlet ($C_L/C_{L0} = 0.5$). The performances of each adsorption test were evaluated by four indicators, referred to a breakpoint concentration of 1 $mg_P\ L^{-1}$ (EU limit for the discharge of WWTPs in surface water, for WWTPs larger than 100,000 people equivalent): i) number of MWW Bed Volumes (BVs) treated at breakpoint (BP); ii) P adsorption yield at BP; iii) sorbent utilization efficiency, i.e. fraction of active sites used at BP; and iv) P operating capacity at BP, i.e. the mean P concentration in the solid (Frascari et al., 2019a, 2019b; Medri et al., 2022). These indicators were calculated as illustrated in Text S4, Supplementary Material. Experimental outlet concentrations were interpolated by means of the Thomas Model (Thomas, 1944), often used for simulating ion exchange processes (Text S5, Supplementary Material). After adsorption, the column was washed with at least 2 BVs of demineralized water fed co-currently. Eventually, the desorption/regeneration procedure was performed by eluting 20 BVs of NaOH 2 % *w*/w to regenerate the sorbent and recover the sorbed anions. The EBCT was set to 10 min. The P desorption performance was evaluated by means of the overall P recovery yield (Text S4, Supplementary Material).

2.6. Analytical methods

All chemicals were provided by Sigma-Aldrich (Milano, Italy). Ion analyses were performed with an Integrion ion chromatograph (TermoFisher Scientific, Walthman, Massachusetts, USA), as described previously (Pinelli et al., 2022a). Average experimental errors, estimated by statistical elaboration of repeated analysis of check standards, resulted 5 % for anion concentration. Total suspended solids, COD and BOD_5 were determined as described previously (Pinelli et al., 2022a). Fe, and Mg were determined according to standard procedures UNI EN ISO 15587-2:2002 and UNI EN ISO 17294-2:2016.

The Anion Exchange Capacity (AEC) of the sorbents was assessed in a 0.1-m column. The sorbent was packed following the Rhom and Haas procedure (Rohm and Hass Company, 2005). The adsorption bed was saturated with phosphate eluting a 1 N synthetic solution of K_2HPO_4 and K_2HPO_4. Then a 1 N NaOH solution was used to displace the adsorbed phosphate. The AEC was assessed as total P desorbed divided by dry sorbent mass.

SEM-EDS analysis on the desorbed product, after precipitation with $Ca(OH)_2$, was performed with a Zeiss EP EVO 50 with different secondary electron detector (High Vacuum, ~10–4 Pa; Variable Pressure, 10-1000 Pa; Environmental Pressure, <3000 Pa) and back scattered electron detector (QBSD). The EDS probe was an Oxford Instruments INCA X-act Penta FET® Precision [z > 4 (Be), resolution 129 eV (MnKα

@ 2500cps)]. It is equipped with INCA Microanalysis Suite Software (version 4.15- issue.18 service pack 5). It allows automatic peak recognitions with reference to internal standards for semi-quantitative analysis. The analysis was carried out in High Vacuum, with EHT = 20KeV, WD = 8.5, SE detector. Area spectra, point spectra and element distribution map at 500 magnification were acquired.

X-ray diffraction (XRD) patterns of the most promising sorbents were recorded with a Ni-filtered Cu Kα radiation (λ = 1.54178 Å) on a Philips X'Pert vertical diffractometer equipped with a pulse height analyzer and a secondary curved graphite-crystal monochromator. The analysis of the phases present in the patterns were performed using Bragg's Law to calculate the crystalline *d* values and comparing them with those reported in literature and collected in the International Centre for Diffraction Data Database. The BET surface area of sorbents was determined by N_2 absorption-desorption at liquid N_2 temperature using a Sorpty 1750 Fison instrument. 0.2 g of the sample was loaded for measurement, and the sample was outgassed at 150 °C before N_2 absorption.

3. Results and discussion

3.1. Single-point equilibrium tests

In order to select the most promising adsorption materials for P-removal from MWW, the 9 materials illustrated in section 2.1 were tested by means of single-point batch tests conducted with the saline Falconara WWTP effluent (Table 1), spiked with a P solution to obtain initial P concentrations equal to 7, 23, 34 and 88 mg L^{-1}. The main results are shown in Fig. 1 in terms of equilibrium sorbed fraction of the P mass initially present in the test, versus equilibrium liquid-phase fraction, so as to allow an easy detection of the most promising materials. No relevant pH variations were detected during the tests.

Fig. 1 shows that the most effective materials resulted calcined Pural 70 and calcined pyroaurite, followed by calcined Pural 70 + Fe_2O_3 and calcined Pural 50. These results indicate that calcination leads to a marked improvement of the P sorption capacities of hydrotalcites. These materials resulted in complete sorption of the P initially supplied in the tests at initial P concentrations of 7 and 23 mg L^{-1}, and in sorbed fractions in the 92–99 % in the tests at initial P levels of 34 and 88 mg L^{-1}. The non -calcined materials Pural 70, Pural 50, pyroaurite and LayneRT resulted in intermediate performances, with sorbed fractions in the 52–84 %, whereas FerroSorp® Plus resulted the least performing material. The better P adsorption performances of the calcined materials can be ascribed to the fact that in the non-calcined LDHs phosphate has to diffuse in the inter-layer space and replace the carbonate and OH^- ions; conversely, the mixed-oxide structure of calcined materials exposes bi- and tri-valent cations which are ready to bind phosphate anions without any need to diffuse between layers or replace other anions.

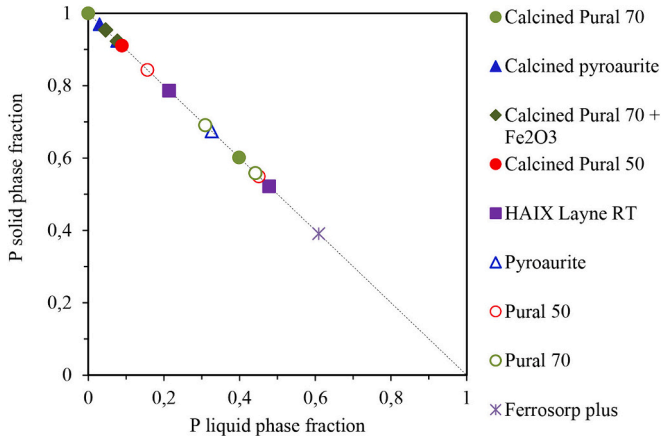

Fig. 1. Main results of the single-point batch tests.

On the basis of these results, calcined Pural 70 and calcined pyroaurite were pre-selected as the most promising P sorbents, for further investigation. As next step, both materials were pelletized at 1.3 t cm^{-2}, sieved in the 0.35–0.71 mm range, packed in 20-cm bed columns and exposed to a mechanical resistance test by flowing water at superficial velocities in the 1–10 m h^{-1} range for 5 h, while monitoring pressure drop. Calcined pyroaurite resulted in a stable condition of the packed bed, with modest pressure drops coherent with those predicted by the Ergun equation (Ergun, 1952). Conversely, calcined Pural 70 rapidly collapsed, resulting in clogging of the packed bed and in a dramatic increase in pressure drop. Calcined pyroaurite was thus selected as the best material, to be further investigated by means of complete isotherms and continuous flow adsorption / regeneration tests.

3.2. Adsorption isotherms

Calcined pyroaurite was further investigated by means of a complete isotherm in the P initial concentration range 2–40 mg_P L^{-1}, using Bologna WWTP effluent. Fig. 2 shows the experimental data obtained with the virgin material and with used calcined pyroaurite sampled from a column after 6 repeated adsorption/regeneration cycles. The pyroaurite isotherms were benchmarked against that previously obtained by the same research group with the same WWTP effluent with LayneRT (Pinelli et al., 2022a), the only sorbent for which the P recovery process has been scaled-up to demonstration scale (10 m^3 d^{-1}) and assessed economically (Guida et al., 2021; Huang et al., 2020). All experimental data were interpolated with the Langmuir and Freundlich models. For calcined pyroaurite Langmuir resulted in a slightly higher R^2, and the best-fitting Langmuir curves and parameters are reported in Fig. 2 for all the sorbents. Fig. 2 shows that calcined pyroaurite features P sorbed concentrations 3 times higher than those of LayneRT, at the P aqueous concentrations typical of MWW. Fig. 2 also illustrates that the P sorption capacities of calcined pyroaurite resulted highly stable during 6 continuous flow adsorption/regeneration cycles conducted with actual MWW (described in section 3.3), a crucial result in the perspective to minimize the process operational cost thanks to a long-term duration of each sorbent load.

The maximum P sorption capacity estimated for calcined pyroaurite with the Bologna WWTP effluent (26 ± 2 mg_P g^{-1}) resulted 3 times higher than that previously estimated for LayneRT with the same effluent (8.7 ± 1.4 mg_P g^{-1}; (Pinelli et al., 2022a)). As shown in Table S2 in Supplementary Material, where the P sorption capacities obtained for several LDHs are reported, to the best of the authors' knowledge, this is the first study in which P sorption capacity was estimated in tests conducted with actual MWW, whereas all previous studies utilized synthetic solutions of phosphate in water, without any effect of competing anions. In the case of LayneRT, it was previously shown that the switch from synthetic phosphate solution to an actual MWW determined a 4.5-fold decrease in maximum P sorption capacity (Pinelli et al., 2022a), confirming the relevant competition exerted mainly by chloride, sulphate and carbonate. As shown in Table S2, despite the use of synthetic phosphate solutions, 6 materials (Mg—Al 4:1 LDH, thermally treated concrete, iron oxide-coated GAC, Zr-loaded Ca-montmorillonite, Zr-modified corn straw, calcined waste egg shells) resulted in maximum P capacities lower than or similar to that estimated here for calcined pyroaurite, whereas 5 LDHs featured higher maximum capacities. Among these, Sun et al. (2013) obtained – in the absence of any competing effect - a 78 mg_P g^{-1} capacity with a calcined pyroaurite similar to that object of this study, coherent with the 26 mg_P g^{-1} capacity obtained in this work with an actual WWTP effluent.

3.3. Continuous flow breakthrough tests conducted with calcined pyroaurite

On the basis of the encouraging isotherm results, calcined pyroaurite

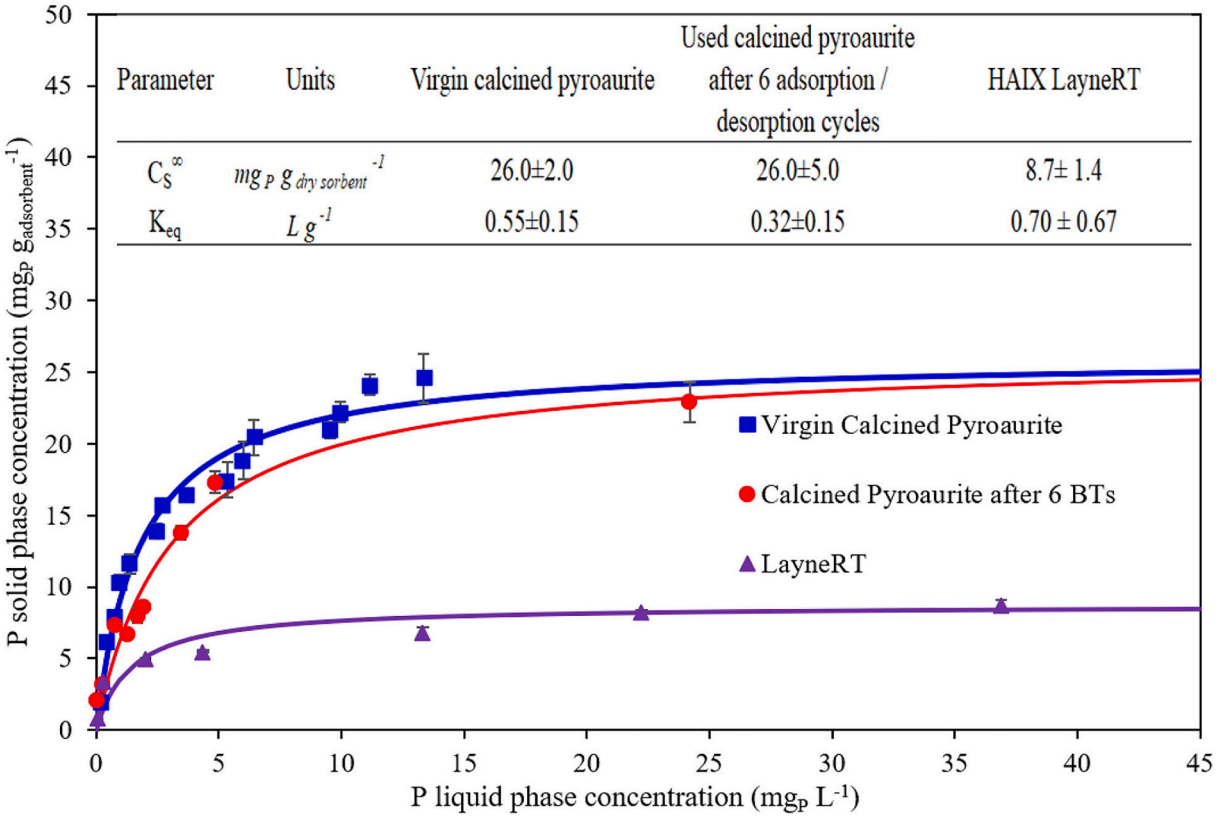

Fig. 2. P adsorption isotherms conducted with virgin calcined pyroaurite (blue squares) and after the operation of 6 adsorption/desorption breakthrough cycles (red circles), using the Bologna WWTP effluent. As benchmark, the P isotherm previously obtained with LayneRT (violet triangles) with the same effluent is reported. For each material, the best fitting Langmuir interpolation is shown (solid line), and the corresponding parameters are reported.

was further investigated by means of repeated adsorption/regeneration cycles conducted with actual MWWs. The process was initially investigated in a 20-cm packed bed, and later scaled-up to a 60-cm packed bed.

3.3.1. Adsorption / desorption breakthrough tests in the 20-cm column

Preliminary fluid-dynamic tests were conducted after column packing, to verify packing quality and column efficiency. Typical experimental curves are shown in Fig. S1, and the packing quality parameters are compared in Table S3, Supplementary Material. Both the asymmetry factor (As, 3.2) and the Height Equivalent of a Theoretical Plate (HETP, 20 mm) indicate the attainment of a satisfactory column packing, with negligible contribution of preferential paths. Further tests conducted after 6 adsorption / desorption assays resulted in similar values of As and HETP (data not shown), providing an important confirmation of the robustness and stability of calcined pyroaurite.

Five consecutive adsorption/desorption breakthrough (BT) tests were then conducted in the 20-cm column with Bologna WWTP effluent (Table 1) spiked at 7 $mg_P\ L^{-1}$ at an empty bed contact time (EBCT) of 5 min, typical for P recovery ion exchange processes (Pinelli et al., 2022a). As a representative example, the adsorption breakthrough curves relative to P and the other competing anions, obtained in the first test, are shown in Fig. 3a. The experimental P BT curve was interpolated by the Thomas model, so as to draw the complete BT curve and to obtain estimates of the sorbent's maximum operating capacity and utilization efficiency. Fig. 3a shows that calcined pyroaurite rapidly released chloride, nitrate and sulphate after about 100 BVs, whereas phosphate started to be released after about 500 BVs. This result shows the high selectivity of calcine pyroaurite for phosphate. As shown in Fig. 3b, phosphate, chloride and sulphate were co-eluted, and P desorption was almost completed after the elution of 20 BVs of NaOH regeneration solution.

To test the stability and robustness of the process of P recovery with calcined pyroaurite, five repeated adsorption/desorption cycles were conducted in the 20-cm column with the same sorbent load, with Bologna WWTP effluent. As shown in Fig. 4, that reports the P adsorption (a) and desorption (b) breakthrough curves relative to the first and last of these cycles, the process resulted stable, with reasonably overlapping curves during both adsorption and regeneration steps. Pressure drops, monitored during both adsorption and desorption, resulted <10 mbar, in good agreement with the Ergun equation, and remained stable throughout the 5 cycles. This indicates that no clogging due to accumulation of MWW suspended solids or fragmentation of the sorbent particles occurred.

The average performance parameters obtained during the 5 repeated cycles are reported in Table 2. These cycles led to promising performances assessed at the 1 $mg_P\ L^{-1}$ breakpoint, in terms of BVs of MWW treated (about 730), sorbent utilization efficiency (69 %), overall P recovery yield (92 %), P operational capacity (OC) (8.1 $mg_P\ g^{-1}$) and P concentration in the desorbed product after 20 BVs of elution with NaOH (242 $mg_P\ L^{-1}$). The Thomas model simulation allowed to estimate also the OC at sorbent saturation, i.e. in equilibrium with the 7 mg L^{-1} P inlet concentration, that resulted 60 % higher than that estimated at the BP. As shown in Table 2, calcined pyroaurite can also comply with the lower P limit imposed by the new Urban WW Directive for plants >150,000 people equivalent (0.5 $mg_P\ L^{-1}$), with a 17 % decrease of the number of BVs treated at the BP.

In order to investigate the last step of the P recovery process, a dose of $Ca(OH)_2$ corresponding to 4 times the molar stoichiometric amount required to precipitate the desorbed P as $Ca_2(PO_4)_3$ was added to the desorbed product obtained from BT5. After 3 h of mixing (120 rpm, 22 °C) the precipitated product was separated by 0.25-μm filtration, dried at 105 °C and subjected to SEM-EDS analysis, which revealed the

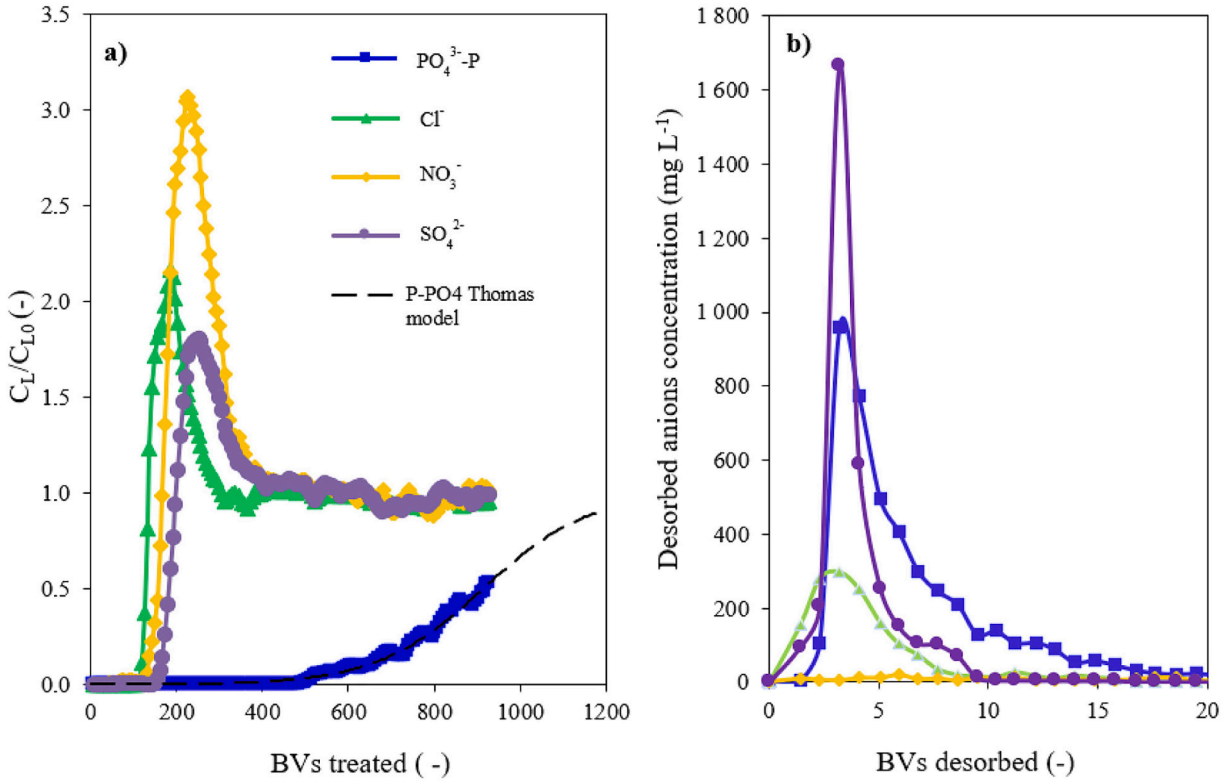

Fig. 3. Adsorption (a) and desorption (b) continuous flow test of BT1 conducted with calcined pyroaurite and Bologna WWTP effluent in the 20-cm plant: breakthrough curves of phosphorous and competing anions and Thomas model simulation of P adsorption curve. In the adsorption curves (a), anion concentrations at the column outlet were normalized to their respective concentrations in the influent $CL_{,0}$ (PO_4^{3-}-P = 7 mg L^{-1}, Cl^- = 150 mg L^{-1}, NO_3^- = 6.7 mg L^{-1}, SO_4^{2-} = 104 mg L^{-1}), to enhance visual clarity of the figure.

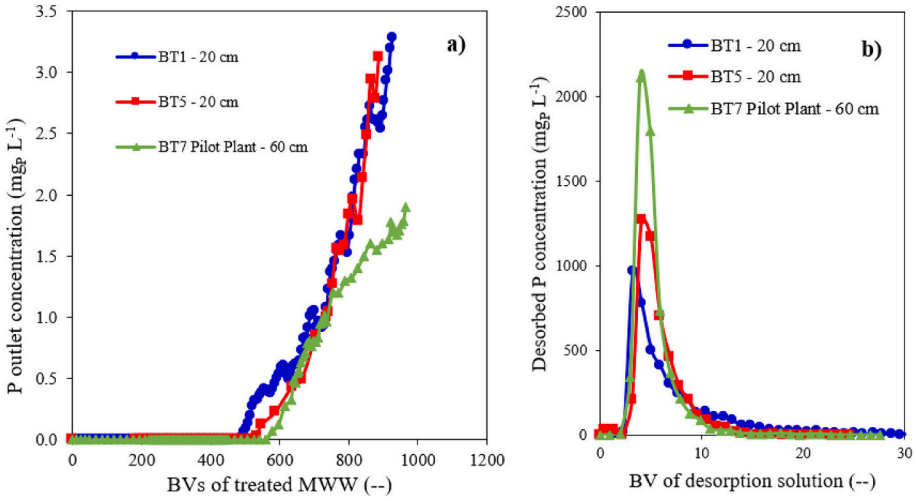

Fig. 4. Adsorption (a) and desorption (b) repeated P breakthrough tests conducted in the 20-cm column (BT 1–5) and in the 60-cm column, with Bologna WWTP effluent spiked at 7 mgP L^{-1}.

presence of oxygen (52 wt%), calcium (33 wt%), phosphorous (7 wt%) and carbonium (8 wt%). The final product can thus be considered to be mainly composed of $Ca_3(PO_4)_2$ - typically used for the production of P-based fertilizers (Huang et al., 2020) - and $CaCO_3$. No traces of chloride, sulfur, iron, magnesium, aluminum or heavy metals were detected, indicating that pyroaurite does not release any Fe or Mg, and that the final precipitated product does not contain any elements that could hinder its use for the production of fertilizers. Furthermore, the concentrations of Fe and Mg in the desorbed product resulted <0.5 mg L^{-1} and < 1 mg L^{-1} respectively, which confirms the absence of Fe and Mg release from pyroaurite.

Finally, the same load of calcined pyroaurite was tested by means of a 6th adsorption / desorption cycle conducted with Falconara WWTP effluent, a saline MWW deriving from a hotspot of seawater intrusion featuring a chloride concentration double than that of the Bologna WWTP effluent (Table 1). As shown in Fig. S2, Supplementary Material, the higher competition exerted by chloride determined an earlier breakthrough of P, resulting in a 56 % decrease in BVs treated and a 55 % decrease in sorbent utilization efficiency (Table 2). However, the P operational capacity at saturation, the overall P recovery and the P

concentration in the desorbed product resulted quite stable. These results indicate that calcined pyroaurite is a robust material that can be effectively used for P recovery also from saline MWW, despite a predictable decrease in specific performances.

3.3.2. Breakthrough tests in the 60-cm pilot plant

In the last part of the work, the process of P recovery with calcined pyroaurite was scaled-up to a bed height of 60-cm located in an automated pilot plant, in order to assess the performance in operating conditions as close as possible to full-scale applications. The scale-up was performed at constant EBCT (5 min adsorption, 10 min desorption), which determined a 3-fold increase in superficial velocity during both steps. As in the 20-cm column, preliminary fluid-dynamic tests were conducted to assess packing quality. As shown in Table S3 and Fig. S1, Supplementary Material, thanks to the 3-fold increase in packed bed height the packing quality resulted better in terms of both asymmetric factor (2.4, versus 3.2 in the 20-cm bed) and HETP (17 versus 20 mm).

As illustrated in Fig. 4a, the adsorption P breakthrough curve resulted delayed in comparison to those obtained in the 20-cm column, coherently with the increase in bed height. As shown in Table 2, the 3-fold increase in bed height determined a slight increase in BVs treated at the 1 mgP L^{-1} BP and in P operational capacity at saturation (that reached 13.4 mgP g^{-1}). Conversely, the overall P recovery yield resulted stable at 93 %. The desorption P curve (Fig. 4b) resulted sharper, with a 97 % recovery of the sorbed P after the elution of just 10 BVs of NaOH 0.5 M. This allowed to achieve a 2-fold increase in P concentration in the desorbed product, that reached 579 mgP L^{-1}, about 80 times higher than the P concentration in the initial MWW feed. Assuming that the regenerant NaOH solution can be reused 8 times (Guida et al., 2021), and considering the NaOH consumption associated to the replacement of the sorbed anions with OH^-, the use of 10 BVs of NaOH in each desorption step corresponds to a final NaOH consumption of about 50 g $m^{-3}_{treated\ WW}$. This represents an acceptable value, in comparison to the typical 40–45 g $m^{-3}_{treated\ WW}$ consumption of $AlCl_3$, the agent typically used for the chemical precipitation of P in traditional WWTPs (Tchobanoglous et al., 2012).

These results indicate that the P recovery process was successfully scaled-up to a 60 cm bed height.

For comparison, a breakthrough test previously carried out with HAIX LayneRT with the same WWTP effluent, at the same EBCT, in a 94-cm column, is shown in Fig. S2 (P adsorption curve) and Fig. S3 (desorption curves of all anions) (Pinelli et al., 2022a). As shown in Table 2, LayneRT resulted in significantly worse performances, with a 65 % decrease in BVs treated at the 1 $mg_P\ L^{-1}$ BP in comparison to the calcined pyroaurite test conducted in the 60-cm column, and a 46 % decrease in P operational capacity at sorbent saturation with the 7 mg L^{-1} P concentration in the inlet MWW. These results are coherent with the significantly higher total anion exchange capacity of pyroaurite (119 ± 17 $mg_P\ g^{-1}$) against that of LayneRT (41 ± 7 $mg_P\ g^{-1}$). On the other hand, LayneRT features a 65 % increase in sorbent utilization efficiency, thanks to the significantly steeper P adsorption curve in comparison to that of calcined pyroaurite. As shown in Fig. S3, Supplementary Material, the LayneRT desorption curves are characterized by a very high peak in sulphate concentration, resulting in a 66 % decrease in P concentration and a much higher sulphate concentration, in comparison to calcined pyroaurite (Table 2).

As for the comparison between the results obtained with calcined pyroaurite and those relative to other LDHs, the assessment of the very limited number of studies that investigated continuous flow P adsorption with LDHs using real MWW confirms the very promising performances of calcined pyroaurite. In a study of P adsorption conducted in a 1.5-cm column packed with a Zr(IV)-Fe(III) LDH, Nuryadin et al. (Nuryadin and Imai, 2021) observed a 47 % decrease in treated BVs at the 1 $mg_P\ L^{-1}$ BP, when they switched from a synthetic P solution to an anaerobic sludge filtrate. In tests conducted with sludge filtrate, they achieved a 1 $mg_P\ L^{-1}$ BP after just 140 BVs (versus 734 in this work) and estimated a 9 $mg_P\ g^{-1}$ operational capacity (versus 12.2 $mg_P\ g^{-1}$). The desorption step conducted with 0.1 M NaOH required 130 BVs (versus 10), and the BVs at constant BP decreased by 50 % during 8 repeated adsorption/desorption cycles. In a study conducted in a 10-cm column packed with calcium aluminate (Cheng et al., 2023), the switch from a P synthetic solution to a real MWW determined a 98 % decrease in P operational capacity, that resulted equal to just 0.44 $mg_P\ g^{-1}$ in the MWW tests, versus 12.2 $mg_P\ g^{-1}$ in this work. During repeated adsorption/desorption cycles, a 50 % decrease in both operational capacity and BVs at constant BP was reported. In a study conducted in a 3-cm column packed with a Zr(IV) modified corn straw, Hu et al. (2020) obtained the 0.5 $mg_P\ L^{-1}$ BP after 420 BVs (versus 600–650 with calcined pyroaurite). These comparisons highlight the importance of testing sorbents with real effluents and to assess their stability over numerous repeated adsorption/desorption cycles.

Even though a complete life cycle assessment of the proposed process of P adsorption / desorption / precipitation is beyond the scope of this paper, it is interesting to compare it with the benchmark process of P recovery as struvite, in terms of consumption of chemicals and indirect greenhouse gas (GHG) emissions. Assuming that the NaOH regenerating solution can be reused up to 8 times (Guida et al., 2021), the P recovery process proposed in this work consumes 7.7 kg of NaOH and 6.3 kg of Ca $(OH)_2$ per kg of P recovered, with corresponding indirect GHG emissions of about 11 $kg_{CO2}\ kg^{-1}_{P\ recovered}$ on the basis of the GHG specific emissions reported by the Ecoinvent 3.10 database (Wernet et al., 2016). Conversely in the case of P recovery as struvite, typically carried out on clarified digestate, P is precipitated with a molar ratio of 1:1:1.2 among phosphate, ammonium, and magnesium. While ammonium is usually present in sufficient concentrations in sludge, Mg^{2+} must be added, commonly as $MgCl_2$. This results in a consumption of 7.9 kg $MgCl_2$ per $kg_{P\ recovered}$ (Hermassi et al., 2018), corresponding to about 14 $kg_{CO2}\ kg_{P\ recovered}^{-1}$, with a 27 % increase in comparison to the alternative process proposed in this work. Furthermore, it should be considered that in most WWTPs P is transferred from MWW to the sludge by precipitation with $AlCl_3$, with a consumption of 6.5 kg $AlCl_3$ per $kg_{P\ recovered}$. Thus, the overall indirect GHG emissions associated to P precipitation with $AlCl_3$ and recovery as struvite are equal to about 23 $kg_{CO2}\ kg^{-1}_{P\ recovered}$, with a 100 % increase in comparison to the innovative process object of this work. In addition, the adsorption / desorption / precipitation technology allows to attain an 80–90 % recovery of the P present in the inlet MWW, whereas in the case of struvite precipitation, P recovery varies in the 7–22 % range (Egle et al., 2015). On the other hand, P desorption from pyroaurite requires the use of NaOH at a pH of about 13.5, which poses safety issues that should be considered in the design of the full-scale process.

3.4. Physio-chemical characterization of the different types of pyroaurite

A first set of XRD analyses was aimed at comparing the chemical structure of virgin non-calcined pyroaurite to those of the other commercial hydrotalcites tested in this work, i.e. Pural 70 and Pural 50. As shown in Fig. S4, Supplementary Material, Pural 70 (Mg/Al atomic ratio = 3, corresponding to the stoichiometric value of the mineral hydrotalcite), shows the most crystalline structure, with sharper and well-defined peaks. Increasing the amount of Al (Pural 50, Mg/Al atomic ratio = 1.3) leads to a loss in crystallinity and a progressive shift of the main peaks towards higher angles, due to the smaller atomic radius of Al compared to Mg. Non-calcined pyroaurite shows all the characteristic peaks of the desired hydrotalcite structure with no segregation of iron oxides, and a slight shift of the signals towards lower angles, related to the bigger atomic radius of Fe compared to Mg and Al.

As shown in Fig. 5, calcination of pyroaurite and the subsequent exposure to MWW (adsorption) and NaOH (desorption) determine deep changes in the sorbent's chemical structure. Calcination of pyroaurite promotes both dehydration and decarboxylation reactions, leading to the formation of a magnesium iron mixed oxide (Mg/Fe/O) with the

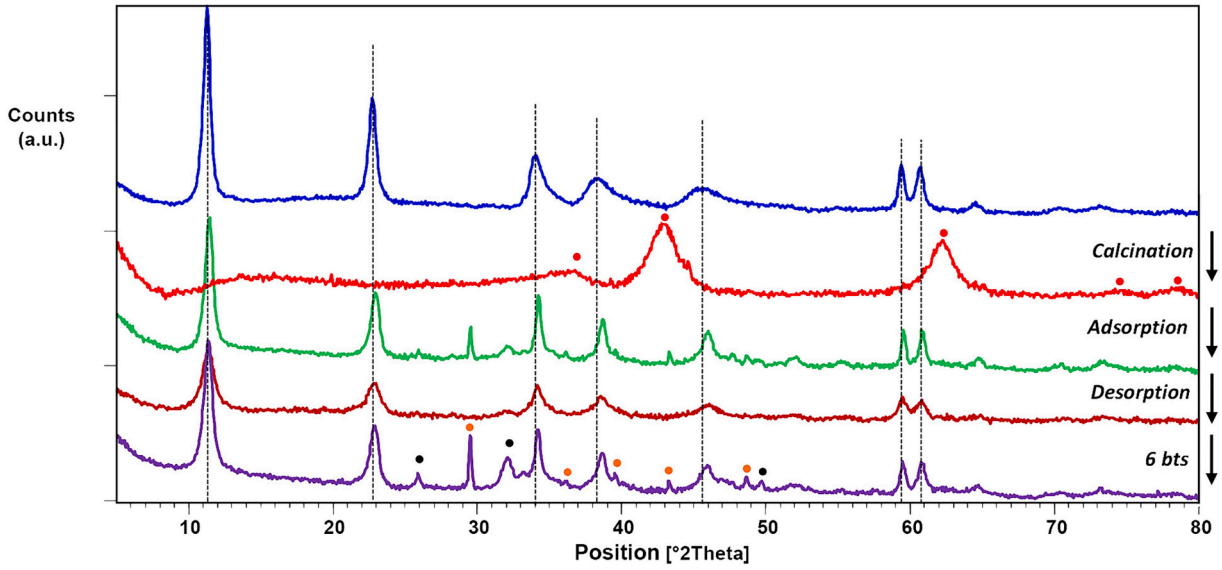

Fig. 5. XRD diffractograms of virgin non-calcined pyroaurite (blue), virgin calcined pyroaurite (red), calcined pyroaurite after one adsorption step (green) calcined pyroaurite after one complete adsorption/desorption cycle (brown) and calcined pyroaurite after 6 adsorption/desorption cycles (purple) The reference patterns are shown as circles; red for MgO structure (PDF. Ref: Code: 01–077-2179), orange for calcite (brown) ($Mg_{0.03}Ca_{0.97}CO_3$, PDF Ref. Code: 01–089-1304) and black for carbonyl hydropxyl apatite ($(C_{a5}PO_4)_{2.5}(CO_3)_{0.5}(OH)$, PDF Ref. Code: 00–019-0272.

same structure of the periclase (MgO), without any evident segregation of other phases (Fig. 5, red curve). The exposure to MWW during adsorption (green curve) leads not only to the restoration of a hydrotalcite-like structure with some shift to higher angles compared to the parent pyroaurite (memory effect of LDHs), but also to the presence of magnesium calcium mixed carbonates (e.g. calcite, $Mg_{0.03}Ca_{0.97}CO_3$) and carbonyl hydroxyl apatite phases (e.g. $Ca_5(PO_4)_{2.5}(CO_3)_{0.5}(OH)$), thanks to the presence of Ca^{2+} in MWW. The restoration of the hydrotalcite structure is mainly ascribable to the incorporation of different counter anions in the interlayer, in particular phosphates, in agreement with the very high selectivity for phosphate shown by calcined pyroaurite. Regeneration conducted with NaOH (brown curve) allows to desorb the adsorbed phosphates, promoting the formation of a proper LDH structure whose surface is completely hydroxylated. The structure of calcined pyroaurite after 6 complete adsorption/desorption cycles (purple curve) resulted highly similar to that observed after just 1 cycle. This represents a relevant confirmation of the reversibility between the LDH structure and the phosphate-rich structure, and ultimately of the stability of this sorbent during repeated adsorption/desorption cycles. This structure is not reported in literature to the best of the authors' knowledge.

The evolution of the pyroaurite structure as a result of calcination, adsorption and desorption was further investigated by measuring the specific surface area (SSA) through Brunauer–Emmett–Teller (BET) analysis. Virgin non-calcined pyroaurite resulted in a relatively low SSA (44 $m^2\ g^{-1}$, versus 180–200 $m^2\ g^{-1}$ of Pural 70 and 50). An increase in SSA was obtained after calcination (+ 43 %), thanks to the removal of water and CO_2 and the reconstruction of the material as a mixed metal oxide with low crystallinity. The first adsorption step, reconstructing the porous hydrotalcite-like LDH structure, led to a further SSA increase, reaching 80 $m^2\ g^{-1}$. The SSA resulted extremely stable after 6 adsorption/regeneration cycles (79 $m^2\ g^{-1}$), providing a further confirmation of the robustness and stability of calcined pyroaurite.

4. Conclusion

The results of the batch and continuous flow tests conducted with two distinct MWWs indicate that calcined pyroaurite is a very promising material for phosphate adsorption and recovery from MWW, thanks to a high P sorption capacity (26 $mg_P\ g^{-1}$ at infinite P concentration, 12 $mg_P\ g^{-1}$ at the typical P level of MWW), the capacity to treat 730 BVs at the 1 $mg_P\ L^{-1}$ breakpoint imposed by the current EU legislation, and a 93 % overall P recovery. Calcium phosphate, largely used for the production of P-based fertilizers, was obtained by precipitation from the desorbed product. The P recovery performances, the chemical structure and the surface area of calcined pyroaurite resulted stable during 5 consecutive adsorption/desorption cycles conducted with actual MWW, indicating the possibility to reuse this sorbent over a high number of cycles. Calcined pyroaurite resulted in satisfactory performances even with a saline MWW deriving from a hotspot of seawater intrusion, confirming the feasibility to implement this P removal/recovery process in coastal areas increasingly affected by saline effluents as a result of climate change. The process scale-up to a 60-cm packed bed, close to the typical column heights of industrial applications, resulted in stable performances, a crucial aspect in the perspective to apply this process at full scale. The proposed process of P adsorption, desorption and precipitation features indirect GHG emissions associated to the consumption of chemicals of about 11 $kg_{CO2}\ kg^{-1}_{P\ recovered}$, with a roughly 50 % reduction in comparison to the emissions resulting from the benchmark process of P chemical precipitation from MWW and recovery from sludge as struvite.

Further research is in progress in order to optimize the adsorption and desorption steps, develop a complete simulation of the multicomponent adsorption process and perform an economic analysis of the proposed process based on a full-scale application.

In the current international context characterized by an increasing drive towards P recovery and a tendency to tighter limits of P concentration in treated wastewaters, the proposed process of P removal / recovery based on calcined pyroaurite can find promising applications not only in case of treated MWW discharge in surface water bodies, but also in case of MWW reuse for managed aquifer recharge, as well as for the treatment of industrial effluents, discharges of combined sewer overflows during rain events and P-rich effluents obtained from municipal sludge dewatering.

CRediT authorship contribution statement

C. Maggetti: Writing – original draft, Investigation, Data curation.

D. Pinelli: Writing – original draft, Supervision, Data curation, Conceptualization. **V. Di Federico:** Writing – review & editing. **L. Sisti:** Writing – review & editing, Methodology. **T. Tabanelli:** Writing – review & editing, Methodology, Conceptualization. **F. Cavani:** Writing – review & editing, Resources. **D. Frascari:** Writing – review & editing, Supervision, Resources, Methodology, Funding acquisition, Conceptualization.

Declaration of competing interest

The authors declare that they have no known competing financial interests or personal relationships that could have appeared to influence the work reported in this paper.

Data availability

Research data underlying this manuscript have been published in the AMS Acta Institutional Research Repository (https://doi.org/10.6092/unibo/amsacta/7759).

Acknowledgments

This work received funding from the European Union's Horizon Europe research and innovation program under grant agreement No 101082048 (MAR2PROTECT project), from the European Commission, NextGenerationEU – Piano Nazionale di Ripresa e Resilienza (PNRR) – Italian Ministry of University and Research (project number PE_00000021) and from the MUR PRIN 2022 grant No 20229THRM2 (GEA project) funded by the European Union – Next Generation EU.

Dataset

Research data underlying this manuscript have been published in the Zenodo Research Repository (DOI: 10.5281/zenodo.13338190).

Appendix A. Supplementary data

Supplementary data to this article can be found online at https://doi.org/10.1016/j.scitotenv.2024.175509.

References

Blaney, L.M., Cinar, S., SenGupta, A.K., 2007. Hybrid anion exchanger for trace phosphate removal from water and wastewater. Water Res. 41, 1603–1613. https://doi.org/10.1016/j.watres.2007.01.008.

Boyer, T.H., Persaud, A., Banerjee, P., Palomino, P., 2011. Comparison of low-cost and engineered materials for phosphorus removal from organic-rich surface water. Water Res. 45, 4803–4814. https://doi.org/10.1016/j.watres.2011.06.020.

Bunce, J.T., Ndam, E., Ofiteru, I.D., Moore, A., Graham, D.W., 2018. A Review of Phosphorus Removal Technologies and Their Applicability to Small-Scale Domestic Wastewater Treatment Systems. Front. Environ. Sci. 6 https://doi.org/10.3389/fenvs.2018.00008.

Cheng, P., Liu, Y., Yang, L., Ren, Q., Wang, X., Chi, Y., Yuan, H., Wang, S., Ren, Y.-X., 2023. Phosphate adsorption using calcium aluminate decahydrate to achieve low phosphate concentrations: batch and fixed-bed column studies. J. Environ. Chem. Eng. 11, 109377 https://doi.org/10.1016/j.jece.2023.109377.

Cipolla, S.S., Maglionico, M., 2014. Heat recovery from urban wastewater: analysis of the variability of flow rate and temperature in the sewer of Bologna, Italy. Energy Procedia 45, 288–297. https://doi.org/10.1016/j.egypro.2014.01.031.

Cumbal, L., Greenleaf, J., Leun, D., SenGupta, A., 2003. Polymer supported inorganic nanoparticles: characterization and environmental applications. React. Funct. Polym. 54, 167–180. https://doi.org/10.1016/S1381-5148(02)00192-X.

De Maron, J., Eberle, M., Cavani, F., Basile, F., Dimitratos, N., Maireles-Torres, P.J., Rodriguez-Castellón, E., Tabanelli, T., 2021. Continuous-flow methyl methacrylate synthesis over gallium-based bifunctional catalysts. ACS Sustain. Chem. Eng. 9, 1790–1803. https://doi.org/10.1021/acssuschemeng.0c07932.

Egle, L., Rechberger, H., Zessner, M., 2015. Overview and description of technologies for recovering phosphorus from municipal wastewater. Resources, Conservation and Recycling 105, 325–346. https://doi.org/10.1016/j.resconrec.2015.09.016.

EPA - U.S. Environmental Protection Agency, 2007. Advanced Wastewater Treatment to Achieve Low Concentration of Phosphorus.

Ergun, S., 1952. Fluid flow through packed columns. Chemical engineering progress 48.

Frascari, D., Bacca, A.E.M., Zama, F., Bertin, L., Fava, F., Pinelli, D., 2016. Olive mill wastewater valorisation through phenolic compounds adsorption in a continuous flow column. Chem. Eng. J. 283, 293–303. https://doi.org/10.1016/j.cej.2015.07.048.

Frascari, D., Molina Bacca, A.E., Wardenaar, T., Oertlé, E., Pinelli, D., 2019a. Continuous flow adsorption of phenolic compounds from olive mill wastewater with resin XAD16N: life cycle assessment, cost–benefit analysis and process optimization. J. Chem. Technol. Biotechnol. 94, 1968–1981. https://doi.org/10.1002/jctb.5980.

Frascari, D., Molina Bacca, A.E., Wardenaar, T., Oertlé, E., Pinelli, D., 2019b. Continuous flow adsorption of phenolic compounds from olive mill wastewater with resin XAD16N: life cycle assessment, cost–benefit analysis and process optimization. Journal of Chemical Technology & Biotechnology 94, 1968–1981. https://doi.org/10.1002/jctb.5980.

European Commission, 2024. Regulation (EU) 2024/1252 of the European Parliament and of the Council of 11 April 2024 establishing a framework for ensuring a secure and sustainable supply of critical raw materials and amending Regulations (EU) No 168/2013. In: (EU) 2018/858, (EU) 2018/1724 and (EU) 2019/1020 (Text with EEA relevance).

Gizaw, A., Zewge, F., Chebude, Y., Tesfaye, M., Mekonnen, A., 2022. A fixed-bed column study of solid waste-based calcium silicate hydrate for the phosphate removal. AQUA - Water Infrastructure, Ecosystems and Society 71, 849–861. https://doi.org/10.2166/aqua.2022.167.

Gjyli, S., Korpa, A., Tabanelli, T., Trettin, R., Cavani, F., Belviso, C., 2019. Higher conversion rate of phenol alkylation with diethylcarbonate by using synthetic fly ash-based zeolites. Microporous Mesoporous Mater. 284, 434–442. https://doi.org/10.1016/j.micromeso.2019.04.065.

Guida, S., Conzelmann, L., Remy, C., Vale, P., Jefferson, B., Soares, A., 2021. Resilience and life cycle assessment of ion exchange process for ammonium removal from municipal wastewater. Sci. Total Environ. 783, 146834 https://doi.org/10.1016/j.scitotenv.2021.146834.

Hermassi, M., Dosta, J., Valderrama, C., Licon, E., Moreno, N., Querol, X., Batis, N.H., Cortina, J.L., 2018. Simultaneous ammonium and phosphate recovery and stabilization from urban sewage sludge anaerobic digestates using reactive sorbents. Sci. Total Environ. 630, 781–789. https://doi.org/10.1016/j.scitotenv.2018.02.243.

Hu, Y., Du, Y., Nie, G., Zhu, T., Ding, Z., Wang, H., Zhang, L., Xu, Y., 2020. Selective and efficient sequestration of phosphate from waters using reusable nano-Zr(IV) oxide impregnated agricultural residue anion exchanger. Sci. Total Environ. 700, 134999 https://doi.org/10.1016/j.scitotenv.2019.134999.

Huang, X., Guida, S., Jefferson, B., Soares, A., 2020. Economic evaluation of ion-exchange processes for nutrient removal and recovery from municipal wastewater. Npj clean. Water 3, 1–10. https://doi.org/10.1038/s41545-020-0054-x.

Keyikoglu, R., Khataee, A., Yoon, Y., 2022. Layered double hydroxides for removing and recovering phosphate: recent advances and future directions. Adv. Colloid Interface Sci. 300, 102598 https://doi.org/10.1016/j.cis.2021.102598.

Kuzawa, K., Jung, Y.-J., Kiso, Y., Yamada, T., Nagai, M., Lee, T.-G., 2006. Phosphate removal and recovery with a synthetic hydrotalcite as an adsorbent. Chemosphere 62, 45–52. https://doi.org/10.1016/j.chemosphere.2005.04.015.

Kwon, D., Kang, J.Y., An, S., Yang, I., Jung, J.C., 2020. Tuning the base properties of mg–Al hydrotalcite catalysts using their memory effect. J. Energy Chem. 46, 229–236. https://doi.org/10.1016/j.jechem.2019.11.013.

Martin, B., Kock, L., Stephenson, T., Parsons, S., Jefferson, B., 2013. The impact of contactor scale on a ferric nanoparticle sorbent process for the removal of phosphorus from municipal wastewater. Chemical Engineering Journal s 215–216, 209–215. https://doi.org/10.1016/j.cej.2012.11.006.

Martin, B.D., Parsons, S.A., Jefferson, B., 2009. Removal and recovery of phosphate from municipal wastewaters using a polymeric anion exchanger bound with hydrated ferric oxide nanoparticles. Water Sci. Technol. 60, 2637–2645. https://doi.org/10.2166/wst.2009.686.

Martin, B.D., De Kock, L., Gallot, M., Guery, E., Stanowski, S., MacAdam, J., McAdam, E. J., Parsons, S.A., Jefferson, B., 2018. Quantifying the performance of a hybrid anion exchanger/adsorbent for phosphorus removal using mass spectrometry coupled with batch kinetic trials. Environ. Technol. 39, 2304–2314. https://doi.org/10.1080/09593330.2017.1354076.

Medri, V., Papa, E., Landi, E., Maggetti, C., Pinelli, D., Frascari, D., 2022. Ammonium removal and recovery from municipal wastewater by ion exchange using a metakaolin K-based geopolymer. Water Res. 225, 119203 https://doi.org/10.1016/j.watres.2022.119203.

Muhammad, A., Soares, A., Jefferson, B., 2019. The impact of background wastewater constituents on the selectivity and capacity of a hybrid ion exchange resin for phosphorus removal from wastewater. Chemosphere 224, 494–501. https://doi.org/10.1016/j.chemosphere.2019.01.085.

Nuryadin, A., Imai, T., 2021. Application of amorphous zirconium (hydr)oxide/MgFe layered double hydroxides composite in fixed-bed column for phosphate removal from water. Global Journal of Environmental Science and Management 7, 485–502. https://doi.org/10.22034/GJESM.2021.04.01.

Ogata, F., Nagai, N., Kishida, M., Nakamura, T., Kawasaki, N., 2019. Interaction between phosphate ions and Fe-mg type hydrotalcite for purification of wastewater. J. Environ. Chem. Eng. 7, 102897 https://doi.org/10.1016/j.jece.2019.102897.

Pan, Bingjun, Wu, J., Pan, Bingcai, Lv, L., Zhang, W., Xiao, L., Wang, X., Tao, X., Zheng, S., 2009. Development of polymer-based nanosized hydrated ferric oxides (HFOs) for enhanced phosphate removal from waste effluents. Water Res. 43, 4421–4429. https://doi.org/10.1016/j.watres.2009.06.055.

Pinelli, D., Bovina, S., Rubertelli, G., Martinelli, A., Guida, S., Soares, A., Frascari, D., 2022a. Regeneration and modelling of a phosphorous removal and recovery hybrid ion exchange resin after long term operation with municipal wastewater. Chemosphere 286, 131581. https://doi.org/10.1016/j.chemosphere.2021.131581.

Pinelli, D., Foglia, A., Fatone, F., Papa, E., Maggetti, C., Bovina, S., Frascari, D., 2022b. Ammonium recovery from municipal wastewater by ion exchange: development and application of a procedure for sorbent selection. J. Environ. Chem. Eng. 10, 108829 https://doi.org/10.1016/j.jece.2022.108829.

Reijnders, L., 2014. Phosphorus resources, their depletion and conservation, a review. Resour. Conserv. Recycl. 93, 32–49. https://doi.org/10.1016/j.resconrec.2014.09.006.

Rohm and Hass Company, 2005. Laboratory Procedures for Testing AmberlystTM and AmberliteTM ion exchange resins and adsorbents.

Schoumans, O.F., Bouraoui, F., Kabbe, C., Oenema, O., Van Dijk, K.C., 2015. Phosphorus management in Europe in a changing world. AMBIO 44, 180–192. https://doi.org/10.1007/s13280-014-0613-9.

Sengupta, S., Pandit, A., 2011. Selective removal of phosphorus from wastewater combined with its recovery as a solid-phase fertilizer. Water Res. 45, 3318–3330. https://doi.org/10.1016/j.watres.2011.03.044.

Sun, X., Imai, T., Sekine, M., Higuchi, T., Yamamoto, K., Akagi, K., 2013. Adsorption of phosphate by calcinated mg-Fe layered double hydroxide. J. Of wat. ˆ|ˆ Envir. Tech 11, 111–120. https://doi.org/10.2965/jwet.2013.111.

Sun, X., Imai, T., Sekine, M., Higuchi, T., Yamamoto, K., Kanno, A., Nakazono, S., 2014. Adsorption of phosphate using calcined Mg3–Fe layered double hydroxides in a fixed-bed column study. J. Ind. Eng. Chem. 20, 3623–3630. https://doi.org/10.1016/j.jiec.2013.12.057.

Tabanelli, T., Cocchi, S., Gumina, B., Izzo, L., Mella, M., Passeri, S., Cavani, F., Lucarelli, C., Schütz, J., Bonrath, W., Netscher, T., 2018. Mg/Ga mixed-oxide catalysts for phenol methylation: outstanding performance in 2,4,6-trimethylphenol synthesis with co-feeding of water. Appl. Catal. Gen. 552, 86–97. https://doi.org/10.1016/j.apcata.2018.01.001.

Tchobanoglous, G., Burton, F.L., Stensel, H.D., Inc, M., E, 2012. Wastewater Engineering: Treatment and Reuse. McGraw-Hill Education.

Thomas, H.C., 1944. Heterogeneous ion exchange in a flowing system. J. Am. Chem. Soc. 66, 1664–1666. https://doi.org/10.1021/ja01238a017.

Wernet, G., Bauer, C., Steubing, B., Reinhard, J., Moreno-Ruiz, E., Weidema, B., 2016. The ecoinvent database version 3 (part I): overview and methodology. Int. J. Life Cycle Assess. 21, 1218–1230. https://doi.org/10.1007/s11367-016-1087-8.